Phys Chem Minerals (2003) 30: 606–614
DOI 10.1007/s00269-003-0343-1

ORIGINAL PAPER

M. Prencipe · M. Tribaudino · F. Nestola

Charge-density analysis of spodumene ($LiAlSi_2O_6$), from ab initio Hartree–Fock calculations

Received: 7 April 2003 / Accepted: 1 July 2003

Abstract An ab initio Hartree–Fock study of spodumene structure has been performed, and the wave function was used for a topological analysis of the electron density. The three non-equivalent oxygen atoms (O1, O2 and O3) of spodumene differed mainly in their valence shell charge concentration (VSCC). In particular, O1 shows a maximum of charge concentration along the Si–O bond path, and two other maxima, which can be regarded as lone pairs, point in the opposite direction with respect to the silicon position. O2 shows a torus of local charge concentration, whose axis is parallel to the Al–Si direction, with a bulge on the external side of the Si–O2–Al angle; even if no maximum exists in the Si direction, the valence shell of O2 appears to be strongly polarized toward the silicon; a slight polarization also exists along the Al–O bond path. A similar situation is displayed by O3, whose charge concentration has a torus-like shape, with the axis parallel to the Si–Si direction, and a bulge on the external side of the Si–O3–Si angle; as in the case of O2, a significant polarization of the valence shell of O3 is observed, towards the two Si directions. By recasting the calculated electron distribution in terms of the valence bond theory, a correlation has been found between structural details (bond lengths) and the hybridization state of the oxygen atoms.

Keywords Spodumene · Hartree–Fock · Electron density

Indroduction

For many years, a wide range of phenomena and facts about reactivity and structure of molecules has been explained or simply described in terms of theories, like the valence shell electron pair repulsion model (VSEPR; Gillespie 1972), whose success is to be sought, on the one hand, in their connection with quantum mechanics and, on the other, with their ability to retain the language and concepts of a more classical view of chemistry. By contrast, crystal chemistry remains essentially tied to classical (that is, non-quantistic) ideas in the attempt to rationalize a large amount of published structural data. One of the central concepts of crystal chemistry is the ionic radius: since the typical bonds in the majority of minerals can be considered to be of ionic nature, the picture of a crystal as an assemblage of spheres (ions) having a definite radius seems to be the most appropriate. However, even if the electron distribution around cations is often almost spherical, that around the anions is not so, and this fact alone makes the very concept of ionic radius difficult. Moreover, there is no doubt that such deviations in the electron density from spherical symmetry, however small, play a key role in determining the strength and other properties of a bond (Bader 1994).

In the attempt to transfer concepts and ideas proper to more advanced branches of chemistry, also to mineralogy, a systematic study of the electron density in minerals has been undertaken (Downs et al. 2002; Gibbs et al. 2001; Prencipe 2002) through the application of the Bader theory (Bader 1994), whose close connections with the VSEPR model, together with its own ability to investigate bond properties, have been clearly demonstrated (Bader 1994; Bader and Heard 1999). As a contribution to this kind of study, the topological properties of the electron density of spodumene ($LiAlSi_2O_6$) were evaluated according to the Bader theory. In turn, the electron density was theoretically calculated by the Hartree–Fock method, which has already been successfully applied in the study of other silicates [e.g. SiO_2 polymorphs: Nada et al. 1990; $MgSiO_3$ with ilmenite and perovskite structure: Nada et al. 1992; D'Arco et al. 1993; pyrope garnet ($Mg_3Al_2Si_3O_{12}$): D'Arco et al. 1996; beryl: Prencipe 2002]. In general, theoretical methods for obtaining the electron density, as an alternative to

M. Prencipe (✉) · M. Tribaudino · F. Nestola
Dipartimento di Scienze Mineralogiche e Petrologiche,
Università di Torino, Via Valperga Caluso 35,
10125 Torino, Italy
e-mail: mauro.prencipe@unito.it
Tel.: +390116707131
Fax: +390116707128

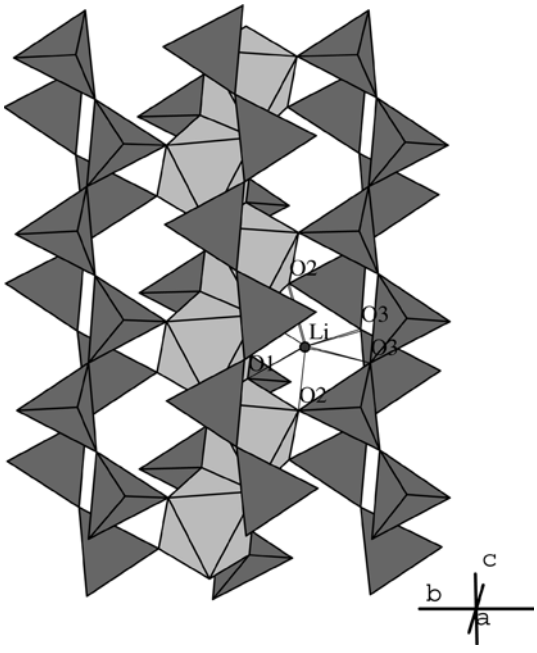

Fig. 1 The spodumene structure viewed along an axis approximately parallel to [100]. For clarity, only one chain of Al-centred octahedra (*light grey*) and only one lithium position have been drawn; Si-centred tetrahedra are in *dark grey colour*

experimental measurements, should be the preferred choice since, on the one hand, the ability of the Hartree–Fock method to provide accurate electron densities is a well-known fact and, on the other hand, experimental (diffraction-based) methods often suffer from various drawbacks (low resolution and truncation effects; anisotropic absorption and extinction effects; difficult deconvolution of thermal motion; biases in the multipolar treatment of data: Volkov et al. 2000) which make the accurate reconstruction of experimental electron densities a difficult task.

Spodumene is a chain silicate belonging to the family of pyroxenes. Its crystal structure (monoclinic, $C2/c$; Cameron et al. 1973) consists of Si-centred tetrahedra, linked at two corners, forming chains along the z axis. These chains are laterally linked by Al-centred octahedra (see Fig. 1) which, in turn, form chains of edge-sharing polyhedra, also running along z. The Li ions occupy cavities formed in the frame of the Si and Al-centred polyhedra. In the structure there are three non-equivalent oxygen ions: O1 which coordinates one Li, two Al and one Si; O2 which is bonded to one Li, one Al and one Si; O3, the bridge between two Si-centred tetrahedra, which coordinates two Si and one Li. The spodumene structure gives us the chance to study how the electron density around the oxygen atoms responds to different coordination environments.

Computational details

Ground-state wave function and energy were calculated ab initio by means of the CRYSTAL98 code (Saunders et al. 1998), which implements the Hartree–Fock (HF), self-consistent field (SCF) method for the study of periodic systems (Pisani et al. 1988). The basis set used for Si and Al (Table 1) is the same as utilized for beryl (Prencipe 2002), after optimization of the exponents of the Gaussian functions representing the outer *sp* and *d* orbitals. Oxygen and lithium were described by 8-411G (Dovesi et al. 1991) and 6-11G (Ojamae et al. 1994) bases, respectively, with optimization of both the exponents of the two outer Gaussian functions for each atom. The thresholds (*ITOL1, ITOL2, ITOL3, ITOL4* and *ITOL5*) controlling the accuracy of the calculation of bielectronic integrals (Saunders et al. 1998) were set to 10^{-7} (*ITOL1* to *ITOL4*) and 10^{-14} (*ITOL5*); these conditions produced a total of 1.6 billion and 65 million of bielectronic and monoelectronic integrals, respectively. The diagonalization of the Fock matrix was performed for six points in the reciprocal space (Monkhorst net; Monkhorst and Pack 1976), for each SCF cycle, by setting the shrinking factor (IS, Saunders et al. 1998) to 2. The threshold for convergence on energy (Saunders et al. 1998) was set to 10^{-6} Hartree.

To test the quality of basis set and wave function, a full geometry optimization was attempted: starting from the experimental fractional coordinates (Tribaudino et al. 2003), the cell parameters were optimized by minimizing the energy with respect to each parameter; however, energy minimum was impossible to achieve as a function of the β angle of the monoclinic cell, probably because of the very small energy variations with such an angle; for this purpose a higher precision of the calculation would be required, which is, at present, not possible due to hardware limitations. Since fully optimized cell parameters were not obtained, fractional coordinates were optimized with the same method (energy minimization) by keeping cell parameters at the experimental values (Tribaudino et al. 2003). Due to convergence problems, it was impossible to apply more sophisticated methods for the optimization (e.g. energy-gradient methods).

Topological properties of the calculated charge density (Bader 1994) were evaluated in the experimental geometry by means of the TOPOND98 program (Gatti 1999); maps of the Laplacian scalar field were realized by means of the P2DCRY97 code (Gatti 1997).

Results and discussion

The comparison with experimental results (mainly from X-ray or neutron diffraction) is here intended only as a means to judge the quality of the calculated wave function. A more detailed discussion will instead regard those aspects not easily accessible to the experimental investigation, in particular those which require an accurate knowledge of the electron density.

The optimized geometry is reported in Tables 2 and 3: a fairly good agreement exists between calculated and experimental (Tribaudino et al. 2003) cell parameters, the differences being lower than 0.7% (however, as stated above, the β was not refined). The calculated cell volume (388.52 Å^3), is also close to the experimental one (388.23 Å^3), being a difference lower than 0.1%. Concerning fractional coordinates, the Li y coordinate shows the largest deviation from the experimental value. This is probably not due to a real effect, like anharmonicity of the potential along the twofold axis (leading to an error in a calculated position which does not take into account zero point and thermal vibrations), since the potential energy curve obtained by calculating the total energy for several Li positions is well interpolated by a quadratic function. Instead, the discrepancy can be due to the very small variations of the total energy as a function of the

Table 1 Basis set. Exponents (α; au^{-1}) and contraction coefficients (c_s, c_p) of the Gaussian type functions, for *s*, *sp* and *d* shells of the various atoms

Shell type	Aluminium			Silicon		
	Exponents	Coefficients		Exponents	Coefficients	
	α	c_s	c_p	α	c_s	c_p
s	70510.0	0.000226		16120.0	0.001959	
	10080.0	0.0019		2426.0	0.01493	
	2131.0	0.0110		553.9	0.07285	
	547.500	0.0509		156.3	0.2461	
	163.100	0.1697		50.07	0.4859	
	54.480	0.3688		17.02	0.3250	
	19.050	0.3546				
	5.402	0.0443				
sp	139.6	−0.0112	0.0089	292.7	−0.002781	0.004438
	32.53	−0.1136	0.0606	69.87	−0.03571	0.03267
	10.230	−0.0711	0.1974	22.34	−0.11500	0.1347
	3.810	0.5269	0.3186	8.150	0.09356	0.3287
	1.517	0.7675	0.2995	3.135	0.6030	0.4496
				1.225	0.4190	0.2614
sp	0.550	1.0000	1.0000	1.079	−0.3761	0.06710
				0.302	1.2520	0.9569
sp	0.430	1.0000	1.0000	0.230	1.0000	1.0000
d	0.533	1.0000		0.568	1.0000	
		Oxygen			Lithium	
s	8020.0	0.00108		840.0	0.00264	
	1338.0	0.00804		217.5	0.00850	
	255.4	0.05324		72.3	0.0335	
	69.22	0.1681		19.66	0.1824	
	23.90	0.3555		5.044	0.6379	
	9.264	0.3855		1.5	1.0000	
	3.851	0.1468				
	1.212	0.0728				
sp	49.43	−0.0883	0.00958	0.55	1.0000	1.0000
	10.47	−0.0915	0.0696			
	3.235	−0.0402	0.2065			
	1.217	0.3790	0.3470			
sp	0.455	1.0000	1.0000	0.25	1.0000	1.0000
sp	0.159	1.0000	1.0000			

Table 2 Calculated (*Calc*) and experimental (*Exp*; Tribaudino et al. 2003) cell parameters (Å). Error on the experimental data, on the last digit, is given *in parentheses*

	a	*b*	*c*	β
Exp	9.504(1)	8.371(1)	5.204(1)	110.33(2)
Calc	9.455	8.366	5.238	–

Li position so that even a small systematic error in the calculation (due, for instance, to basis set inadequacy) can significantly affect the result. Indeed, by interpolating the energy through the expression

$$E = E_0 + \frac{1}{2}K(y - y_0) \quad , \tag{1}$$

where y_0 (absolute coordinate) is the equilibrium position of Li and E_0 the corresponding energy, the value of K was 0.193(3) Hartree Å^{-2} (the error in the last digit comes from the quadratic fitting of the energy versus the y coordinate), to be compared with the much higher value [1.586(5) Hartree Å^{-2}] for Al. The reasonableness of such values of the K constant can be established by calculating the frequencies of vibration of the two ions along the twofold axis (in the limit of the harmonic model): the resulting frequencies are 1.36×10^4 GHz (450 cm^{-1}) and 1.98×10^4 GHz (660 cm^{-1}) for Li and Al, respectively. Such frequencies are in reasonable

Table 3 Calculated (*Calc*) and experimental (*Exp*; Tribaudino et al. 2003) fractional coordinates. Errors on the experimental data are of the order of 10^{-5}

	x	y	z	x	y	z
		Li			Si	
Exp	(0.000)	0.27346	(0.250)	0.29393	0.09366	0.25732
Calc	(0.000)	0.2679	(0.250)	0.2948	0.0933	0.2585
		Al			O1	
Exp	(0.000)	0.90697	(0.250)	0.10971	0.08265	0.14130
Calc	(0.000)	0.9070	(0.250)	0.1110	0.0811	0.1390
		O2			O3	
Exp	0.36460	0.26744	0.30009	0.35656	−0.01463	1.06089
Calc	0.3667	0.2676	0.2959	0.3552	−0.01414	1.0608

agreement with those observed in Raman spectra of spodumene, whose absorption bands in the range 200–600 cm^{-1} (Caltech Mineral Spectroscopy Database 2001) could be tentatively assigned to the Li–O and Al–O vibrations, in analogy with the assignments to *M*–O vibrations in $LiFeSi_2O_6$ (Zhang et al. 2002).

Topological properties of the electron density: bond-critical points

The topological properties of the electron density (Bader 1994) have been evaluated at the experimental geometry determined from neutron diffraction at low temperature (54 K) (Tribaudino et al. 2003). Main results are reported in Table 4. Concerning the properties at the (3, −1) bond-critical points (BCP), results are in line with those reported in literature for ionic and silicate systems (Downs and Swope 1992; Downs 1995; Gibbs et al. 1994, 1997, 1998, 2001; Kirfel and Gibbs 2000; Prencipe 2002). In particular, the bond-critical radius of oxygen [r_b(O)] increases with the electropositivity of the cation to which it is bonded; this is consistent with earlier findings by Feth et al. (1993), who showed a correlation between electronegativity of the cation and the bonded radius of the oxide anion. It is to be noted that within each set of bonds with the same cation r_b(O) increases with the internuclear distance. The bond-critical radii of the cations [r_b(M)] also increase with the *M*–O distances, the variation being more marked in Li [$\Delta r_b(M)/\Delta d_{M-O} \approx 0.32$] than in Al (0.30) and Si (0.26). It is interesting to note that the average bond-critical radius of Li (0.81 Å) is not so different from the ionic radius in sixfold coordination (0.74 Å; Shannon and Prewitt 1969); a larger difference is, however, recorded for Al (0.79 vs. 0.53 Å) and Si (0.66 vs. 0.26 Å); this is connected to the fact that the constant radius of 1.40 Å for the oxide anion, chosen by Shannon and Prewitt (1969), is close to the average r_b(O) critical radius along the Li–O bond (1.39 Å), whereas it is significantly larger than the average critical radii along Al–O (1.13 Å) and Si–O (0.96 Å).

The value of the Laplacian at the BCP [Table 4; $\nabla^2\rho(\vec{r}_c)$] is also an indication of the nature of the interaction (Bader 1994) between two atoms: positive values would indicate closed-shell interactions (ionics fall in this category), whereas negative values indicate shared interactions (covalent bonds). However, concerning the Si–O case, much debate exists in literature about such interpretation; in particular, it is questioned by Gibbs (Gibbs et al. 1998) that the Si–O bond is more covalent than the value of the Laplacian at the BCP would suggest; in fact, following Bader (1994), a certain covalency of this bond would be indicated by either the decrease of r_b(O) as the internuclear distance shortens, or the value of $\rho(\vec{r}_c)$, which is considerably higher than that observed in other ionic interactions. These features contrast with the behaviour of the Laplacian at the critical point, which is positive and increases with the shortening of the Si–O distance (increase in ionicity), as indeed observed also in the case of spodumene (Table 4). On this ground, Gibbs (Gibbs et al. 1998) cast some doubts on the validity of the Bader criteria (B&E criteria; Bader and Essén 1984) for the classification of chemical bonds; in particular, Gibbs questioned the use of the Laplacian for the purpose. Nevertheless, it is clear from the data of Table 4 that, even in the case of Li–O interactions, the critical radius of oxygen decreases by a large amount with the shortening of the internuclear distance and, if one agrees on the fact that the Li–O bond is fully ionic, no matter how far apart Li and O are, then the behaviour of r_b(O) with the *M*–O distance cannot necessarily be taken as an indication of covalency, at least if one considers the dependence of r_b(O) from d_{M-O}, with fixed *M*.

In all of the three cases Si–O, Al–O and Li–O, the positive value of the Laplacian at the critical point is interpreted as the consequence of the higher tendency of the electrons to locally concentrate in the attraction basin of each atom involved, compared to their tendency to locally concentrate in the internuclear region. In fact, the attraction toward the nuclei, with a consequent local depletion of charge concentration from the interatomic region, is measured by the (positive) curvature of the electron density along the internuclear axis (the eigenvalue of the Laplacian field associated with the eigenvector oriented along that axis; λ_3 in Table 4), whereas the tendency of electrons to locally concentrate in the interatomic region is measured by the (negative) curvatures of the electron density in a plane for the critical point normal to the bond path ($\lambda_{1,2}$, Table 4).

Table 4 Bond distance (d_{M-O}), critical radii of cations and oxygen [$r_b(M)$ and r_b(O), respectively] in Å; electron density at the bond-critical point [$\rho(\vec{r}_c)$, in $eÅ^{-3}$]; Laplacian of the electron density [$\nabla^2\rho(\vec{r}_c)$, in $eÅ^{-5}$] and eigenvalues of the Hessian matrix ($\lambda_{1,2}$ and λ_3, in $eÅ^{-5}$) at the same point. Ellipticity ($\epsilon = |\lambda_2/\lambda_1 - 1|$)

Bond	d_{M-O}	$r_b(M)$	r_b(O)	$\rho(\vec{r}_c)$	$\nabla^2\rho(\vec{r}_c)$	$\lambda_{1,2}$	λ_3	ϵ
Li–O1 x2	2.090	0.774	1.316	0.13	3.66	−0.74	5.15	0.027
Li–O3 x2	2.245	0.829	1.416	0.08	2.29	−0.41	3.11	0.121
Li–O2 x2	2.272	0.830	1.442	0.08	2.23	−0.37	2.97	0.154
Al–O2 x2	1.822	0.762	1.061	0.50	13.49	−3.21	19.93	0.017
Al–O1a x2	1.941	0.796	1.144	0.37	9.30	−2.20	13.70	0.020
Al–O1b x2	1.995	0.814	1.181	0.32	7.75	−1.80	11.35	0.016
Si–O2	1.585	0.654	0.932	1.05	27.85	−7.41	42.67	0.006
Si–O3a	1.623	0.665	0.958	0.93	24.31	−6.68	37.67	0.015
Si–O3b	1.626	0.666	0.960	0.93	23.91	−6.62	37.17	0.021
Si–O1	1.644	0.669	0.975	0.93	21.80	−6.44	34.68	0.013

Several O–O (3,-1) BCPs have been found. One is located on the O3–O3 axis, connecting two oxygens from facing tetrahedral chains, in the plane defined by the two oxygens and the Li they coordinate (point *p*1 in Fig. 2). The O3–O3 distance is 2.753 Å; the BCP is on the twofold axis and it is exactly midway between the oxygens (at 1.377 Å from each one), with $\rho(\vec{r}_c) = 0.10$ eÅ^{-3} and $\nabla^2\rho(\vec{r}_c) = 1.72$ eÅ^{-5}; the curvature of the electron density along the O3–O3 axis (λ_3) is 2.35 eÅ^{-5}, whereas the average of curvatures in the plane normal to the same axis ($\lambda_{1,2}$) is -0.31 eÅ^{-5}, with a relatively small value of ellipticity ($\epsilon = |\lambda_1/\lambda_2 - 1| = 0.066$).

Another BCP is present between the O3 atoms: it is located at the intersection of the O3–O3 interaction line with the Si–Si axis, the latter ions belonging to facing tetrahedral chains (point *p*2 in Fig. 2). In this case, the O3–O3 distance is 3.016 Å; the values of the electron density and of the Laplacian at the critical point are 0.05 eÅ^{-3} and 0.98 eÅ^{-5}, respectively ($\lambda_{1,2} = -0.13$ eÅ^{-5}, $\lambda_3 = 1.26$ eÅ^{-5} and $\epsilon = 0.19$).

A BCP point also exists in between two O1 atoms, at the midpoint of the shared edge between two Al-centred octahedra. The O1–O1 distance is 2.509 Å; electron density and Laplacian at the critical point are 0.20 eÅ^{-3} and 3.41 eÅ^{-5}, respectively ($\lambda_{1,2} = -0.39$ eÅ^{-5}, $\lambda_3 = 4.20$ eÅ^{-5}). Compared to the other O–O interactions, in this case the value of ellipticity is remarkably high (11.04) due to the small value of the curvature along the Al–Al direction ($\lambda_2 = -0.06$ eÅ^{-5}, to be compared with $\lambda_1 = -0.73$ eÅ^{-5}); a tentative explanation of this fact could be found in the role played by the Al ions, which are close to the BCP (1.516 Å), so that they can exert an attractive force on the electrons, thus diminishing the curvature of the electron density in the BCP–Al direction. On the other hand, the low value of λ_2 is compensated by a relatively high value of λ_1, so that the mean value of the curvature ($\lambda_{1,2}$) is high enough to assure a sufficiently high concentration of electrons in the interatomic region to shield the repulsion between the nuclei.

The values of the topological parameters observed in the case of the O–O interactions are in line with those reported from other authors (see, for instance, Gibbs et al. 2000 and references therein). Some debate exists in literature about the nature of such an interaction (Abramov 1997; Bader 1998; Tsirelson et al. 1998; Gibbs et al. 2000), in particular about its possible bonding character. It is our opinion that this debate arose from a questionable interpretation of what the existence of a critical point between two nuclei would imply: whenever the attraction basins of two atoms are in contact, a BCP between them must exist (Bader 1994); in this case an atomic interaction line is always found; in order for this interaction to be considered a bonded one (so that we can talk of bond path instead of the more general atomic interaction line), some conditions must be met (Bader 1994): following Berlin (1951), the electronic charge in the binding regions around the two atoms must exceed that accumulated in the antibinding regions. While, in the present case, it is difficult to verify the bonding character following Berlin's criterion (which was derived for a biatomic system), according to the B&E criteria (Bader and Essén 1984), it is clear from our data that, at least in the case of spodumene, the O–O interaction can be classified as a closed-shell one, and it should not be considered a bonded interaction (of the type found, for instance, between cations and anions in

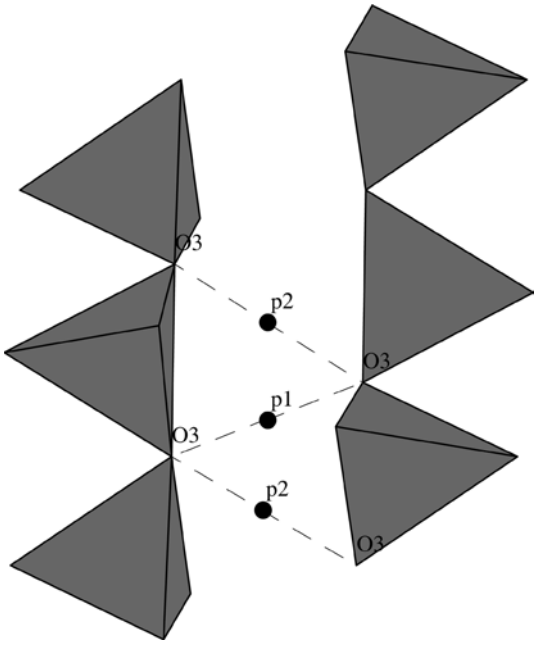

Fig. 2 View of a section of two facing Si-centred tetrahedral chains, showing the positions of the *O3–O3 critical points* (*p1* and *p2*; see text for explanation)

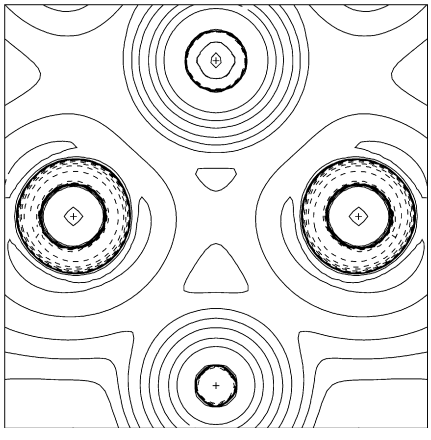

Fig. 3 Map of the Laplacian scalar field on the plane for two O1 atoms (*at the left and right sides*) and for the aluminium ions of the two edge-sharing octahedra. Contour levels at $\pm 2, \pm 4$ and $\pm 8 \times 10^{-n}$ au, with $n = 0, \ldots, -3$. *Dashed lines* refer to negative values of the Laplacian

ionics), since no polarization of the electronic charge of one atom towards the other is infact observed (Fig. 3).

Valence shell charge concentration

The valence shell charge concentration (VSCC) model of an atom is a description of its charge distribution in terms of the properties of the function $L(\vec{r}) = -\nabla^2\rho(\vec{r})$, and it has been shown (Bader 1994) to be strictly related to the valence shell electron-pair repulsion model (VSEPR; Gillespie 1972) widely popular among chemists. In particular, maxima in $L(\vec{r})$ would correspond to maxima in charge concentration, that is, to points where the charge density is higher than the average in the surrounding region. It must be stressed that a maximum in $L(\vec{r})$ does not necessarily indicate a maximum in $\rho(\vec{r})$.

Several maxima [(3,−3) points] in the function $L(\vec{r})$ have been found, all lying around the oxygens. If located far from bond paths, such maxima are generally interpreted as lone pairs (Bader 1994). The function $L(\vec{r})$ shows three maxima around O1; two of them (*lp*1 and *lp*2) display features which are typical for lone pairs of oxygen (Bader 1994; Prencipe 2002) as regards distance from the nucleus, 0.36 Å for both, and the three principal values of curvature: a very sharp profile along the O1–*lp* direction ($\lambda_1 = -360$ au and −330 au, for *lp1* and *lp2*, respectively; 1 au being 86.06 eÅ^{-7}) and a more diffuse shape in the plane normal to O1–*lp* ($\lambda_{2,3} = -4.7$ au and −2.6 au, for *lp*1 and *lp*2, respectively). Even if *lp*1 lies in the direction of the Li ion (the angle O1–*lp*1–Li being almost straight: 174°) and is, therefore, located very close to the Li–O1 bond path, it could be considered a lone pair, due to its features and the similarity with *lp*2. The angle *lp*1–O1–*lp*2 is 151° and *lp*2 is located just above the plane for O1, Al1 and Al2 (see Fig. 4), the angle of the vector O1–*lp*2 with such a plane being 45°. Following Berlin (1951), *lp*2 should play a role in the Al–O1 bond, whereas *lp*1 would exert its influence over the Li–O1 bond, both being located in the relevant binding regions.

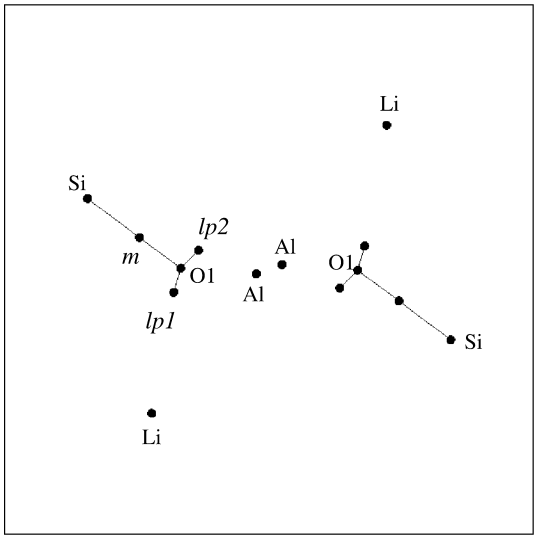

Fig. 4 Positions of the maxima of charge concentration (*lp*1, *lp*2 and *m*) around the *O1 atom*. The two oxygens in the figure are those belonging to the shared edge of the two octahedra, whose central *Al ions* are also drawn

The third maximum in $L(\vec{r})$ around O1, indicated with *m* in what follows, is located along the Si–O1 bond path (see Fig. 4). It is well inside the attraction basin of the oxygen, at about 0.25 Å from the O1–Si BCP, the O1–*m* distance being 0.73 Å. The angles *m*–O1–*lp*1 and *m*–O1–*lp*2 are 110° and 98°, respectively; the O1 nucleus and the three maxima in $L(\vec{r})$ are almost coplanar, for the distance of O1 from the plane for *lp*1, *lp*2 and *m* is only 0.02 Å. Values of curvature of the Laplacian of the electron density, in *m*, are −1.77 au (along an axis approximately coincident with the O1–Si direction), −1.04 and −0.99 au (in the plane, for *m*, normal to the Si–O1 axis); it is to be noted that the curvature along the O1–*m* direction is very much lower than those along O1–*lp*s.

The situation around O2 is different in that such oxygen shows only one lone pair (*lp*) on the external side of the angle Al–O2–Si, at 0.36 Å from the O2 nucleus; the angle of the vector *lp*–O2 with the plane for Al, Si and O2 is 0.4°, so that *lp* is almost coplanar with the three atoms. The *lp* profile is very sharp in the O2–*lp* direction (curvature: −357 au), more relaxed in a direction lying almost in the plane Al–O2–Si (curvature: −7 au) and rather diffuse in the direction normal to such a plane (curvature: −1 au). Even if no maximum has been found along the Si–O2 bond path, the electron density of O2 appears to be polarized in the Si direction. A small polarization is also observed along the Al–O2 bond.

The last oxygen (O3), the bridge between two silicon-centred tetrahedra, has one lone pair (*lp*) located on the bisector of the Si–O3–Si angle, on the external side of it, and at 0.35 Å from the O3 nucleus; the *lp*–O3 vector forms an angle of 26° with the plane for the two Si and O3. The curvature along the *lp*–O3 direction is −375 au, whereas it is −9 au and −1 au along a direction in the Si–O3–Si plane and one normal to the latter, respectively. No maxima of $L(\vec{r})$ were found along the Si–O3 directions but, as in the case of O2, the electron density is polarized toward the silicon ions.

Such results can be recast in the framework of the valence-bond theory (VB); in particular the electron distribution around O1 is consistent with a hybridization scheme close to *sp*; the *lp*1 and *lp*2 lone pairs would be interpreted as the two *sp* lobes, since the angle *lp1*–O1–*lp2* (151°) corresponds to orbitals with 53% of *p* character. In the case of ideal *sp* hybridization, a symmetrical torus of local charge concentration is expected to occur around the axis for the two *sp* lobes; in the case of O1, such a torus in not symmetrical, due to the deviation from the *sp* hybridization, and shows a prominent bulge along the Si–O1 axis.

Less clear is the case of O2 but, by considering the angles of the lone pair with the Si–O2 and Al–O2

directions (112° and 100°, respectively), the Al–O2–Si angle (150°) and the rather different values of curvature in the plane for *lp*, normal to the *lp*–O2 direction, probably the best is to consider an *sp* hybridization, with the two *sp* lobes pointing toward Si and Al; in this case, a torus of charge concentration would exist, with a bulge on the external side of the Al–O2–Si angle (since the *sp* hybridization is not ideal). It should be noted that the function $L(\vec{r})$ also exibits a (3, −1) critical point (*p*) located almost in the plane for O2, Si and Al on the inner side of the Si–O2–Al angle; the curvature along O2–*p* (−314 au) is close to the correspondent found for *lp* (see above); the other two principal curvatures are −3 au and 0.4 au, in a direction lying approximately in the Si–O2–Al plane and in a direction normal to the latter, respectively. In other words, *p* is a maximum of $L(\vec{r})$ in the plane for Si, O2 and Al, whereas it is a minimum (rather smooth) in the direction normal to it; this is consistent with the deformation of the torus of charge concentration around O2, whose axis is parallel to the Si–Al direction, to form a maximum (*lp*) on the opposite side of *p*, with respect to O2. The atomic quadrupolar polarization (traceless) tensor describes the deviation from the spherical symmetry of the atomic charge density (Bader 1994). The three eigenvalues (moments) of the tensor are null if the charge density is spherical; for a sphere flattened at the poles of a reference (*z*) axis, the moment along *z* (Q_{zz}) is positive (oblate spheroid), whereas Q_{zz} is negative for a prolate (that is, elongated along the *z* axis) spheroid. In the case of O2, the tensor corresponds to an oblate spheroid whose relevant axis is parallel to the Si–Al direction; this is consistent with an *sp* hybridization scheme (Bader 1994), with the two *sp* lobes pointing along the Si-Al axis.

The situation around O3 can again be classified as a case of *sp* hybridization, with the two *sp* lobes pointing toward the two silicons; however, since the angle Si–O3–Si is only 138°, such lobes have 57% of *p* character and the torus of charge concentration, whose axis (for O3) is parallel to the Si–Si direction, is therefore strongly asymmetrical, showing the maximum on the external side of the Si–O3–Si angle. In fact, the profile of the charge concentration, for such a maximum, in the direction normal to the Si–O3–Si plane is less diffuse (curvature −1 au) than the correspondent in beryl (Prencipe 2002; Si–O1–Si angle of 170°, curvature −0.4 au), whereas the curvatures in the direction parallel to the Si–Si axis are almost identical in beryl and spodumene. The atomic quadrupole polarization tensor exibits the same behaviour as for O2, since it corresponds to an oblate spheroid whose axis is parallel to the Si–Si direction.

To be noted is the behavior of the $L(\vec{r})$ function around the oxygens, along the Si–O bond axes: a maximum exists only when the Si–O distance is considerably large (Si–O1: 1.644 Å); as such distance decreases, the maximum disappears and the only feature which

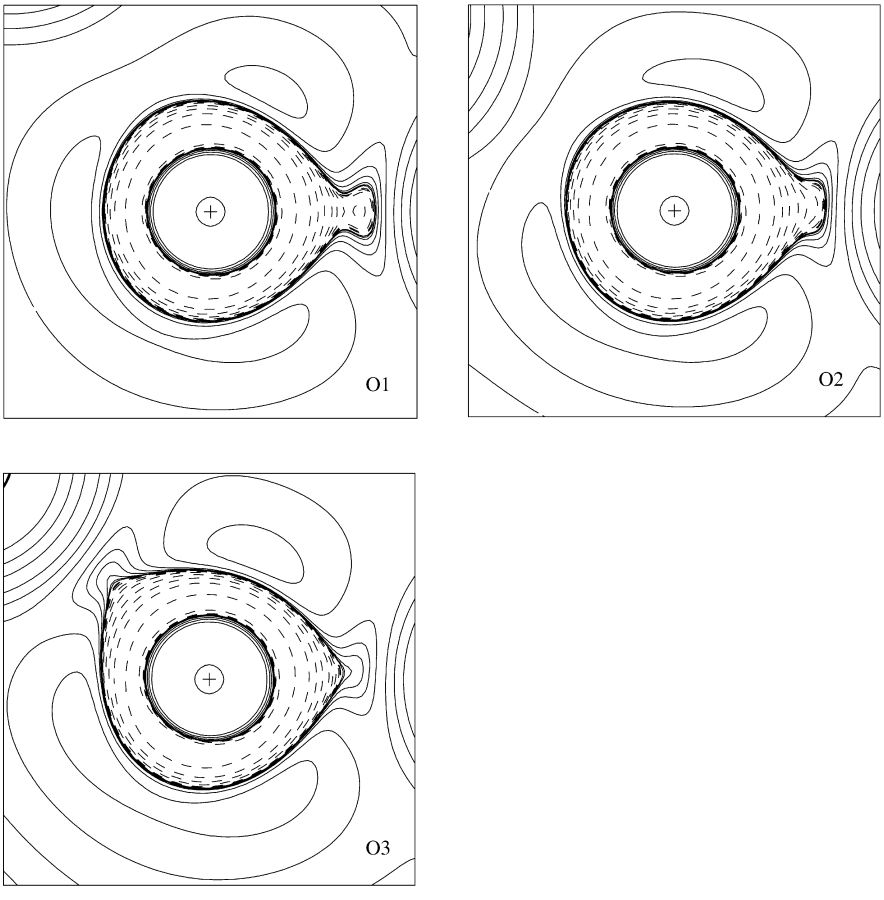

Fig. 5 Maps of the Laplacian scalar field around *O*1, *O*2 and *O*3. The planes chosen are for O1, Si (on the *right side* of the map) and Al (*upper left corner*); O2, Si (*right*) and Al (*upper left*); O3 and the two Si ions it coordinates. Contour levels as in Fig. 3

remains is a polarization of the charge concentration toward Si (see Fig. 5), whose magnitude is larger if the oxygen is bonded to one silicon only (O2) than in the case of bonding with two Si ions (O3).

Electron distribution and structural details

A correlation can be observed between hybridization of oxygen and the Si–O bond lengths (Table 4): the largest distance is Si–O1 where, according to the interpretation given above, the oxygen orbital along that bond is largely *p* in character; the distance decreases in Si–O3 and Si–O2 (57 and 53% of *p* character, respectively). The same correlation was observed in beryl (Prencipe 2002). The correlation is explained by considering the larger penetration of the *s* orbital with respect to the *p*, so that *sp* hybrids form shorter bond lengths than orbitals with less *s* character (Newton and Gibbs 1980; Boisen and Gibbs 1987; Prencipe 2002). Similar considerations can also be drawn for Al–O and Li–O distances; in particular, the hybridization scheme proposed is consistent with the observed Al–O2 distance, which is considerably shorter than the Al–O1 ones (Table 4). As concerns Li, the shorter distance (Li–O1, Table 4) is consistent with the observation of an *sp* lobe belonging to O1, directly pointing toward Li. The Li–O1 distance is significantly shorter than the ideal one (2.14 Å), based on the sum of the Shannon and Prewitt (1969) ionic radii (0.74 and 1.40 Å for the lithium and the oxide ions, respectively); this fact, together with the presence of the lone pair directed toward Li, would suggest a situation similar to that found in the H–O hydrogen bond.

Even apart from considerations based on hybridization, it is clear that a correlation exists between bond distances and electron distribution. This suggests an alternative to more classical ideas based on Pauling's valence bond rule (Pauling 1940; Brown and Shannon 1973) that, beyond having some empirical character, move from models which are no longer tenable: the classical view of an ionic compound as an assemblage of spherical charged particles is inconsistent with the more recent quantum-mechanical description of ionic interactions made by Bader (1994). Moreover, anionic charges derived from the application of the Pauling's valence bond rule (q_P in Table 5; Pauling 1940) or other more refined methods which take *M*–O distances into account (q_{BS}, Brown and Shannon 1973; q_H, Hoppe et al. 1989), foresee differences in the charges of the three oxygens; by contrast, the charges obtained from the integration of the electron density in the attraction basin of each nucleus (q_B, Bader 1994) are almost identical for the three oxygens. It is also interesting to note the similarity between the latter charges and those derived for the two inequivalent oxygens in beryl ($Al_4Be_6Si_{12}O_{36}$): −1.73 e and −1.75 e (Prencipe 2002). These points suggest that, more than the charges, what really distinguishes different oxygens are details in the electron density distribution. Therefore, some doubts are cast on the interpretation of structural details based upon models strongly relying on differences in anionic charges, which are indeed not observed when more sophisticated quantum-mechanical methods are applied.

Table 5 Charges (in electrons) of oxygen ions calculated by the application of Pauling's valence bond rule (q_P; Pauling 1940); the Brown and Shannon method (q_{BS}; Brown and Shannon 1973); the Hoppe method (q_H; Hoppe et al. 1989) and by integration of the charge density over the attraction basin of each oxygen (q_B; Bader 1994)

	q_P	q_{BS}	q_H	q_B
O1	−2.17	−2.00	−1.97	−1.75
O2	−1.67	−1.89	−1.92	−1.74
O3	−2.17	−2.15	−2.11	−1.73

Acknowledgements This work was supported by the National Project Transformations, reactions, ordering in minerals (MIUR, Roma)

References

Abramov YA (1997) Secondary interactions and bond critical points in ionic crystals. J Phys Chem (A) 101: 5725–5728

Bader RFW (1994) Atoms in molecules. International series of monographs in chemistry 22. Oxford University Press, Oxford

Bader RFW (1998) A bond path: a universal indicator of bonded interactions. J Phys Chem (A) 102: 7314–7323

Bader RFW, Essén (1984) The characterization of atomic interactions. J Chem Phys 80: 1943–1960

Bader RFW, Heard GL (1999) The mapping of the conditional pair density onto the electron density. J Chem Phys 111: 8789–8798

Berlin T (1951) Binding regions in diatomic molecules. J Chem Phys 19: 208–213

Boisen MB, Gibbs GV (1987) A method for calculating fractional *s*-character for bonds of tetrahedral oxyanions in crystals. Phys Chem Miner 14: 373–376

Brown ID, Shannon RD (1973) Empirical bond-strength-bond-length curves for oxides. Acta Cryst (A)29: 266–282

Caltech Mineral Spectroscopy Database (2001) The Thermo Galactic web page URL http://spectra.galactic.com/SpectraOnline/Default_ns.htm

Cameron M, Sueno S, Prewitt CT, Papike JJ (1973) High-temperature crystal chemistry of acmite, diopside, hedenbergite, jadeite, spodumene and ureyte. Am Mineral 58: 594–618

D'Arco Ph, Sandrone G, Dovesi R, Orlando R, Saunders VR (1993) A quantum-mechanical study of the perovskite structure type of $MgSiO_3$. Phys Chem Miner 20: 407–414

D'Arco Ph, Freyria Fava F, Dovesi R, Saunders VR (1996) Structural and electronic properties of $Mg_3Al_2Si_3O_{12}$ pyrope garnet: an ab initio study. J Phys Condens Matter 8: 8815–8828

Dovesi R, Roetti C, Freyria Fava C, Prencipe M, Saunders VR (1991) On the properties of lithium sodium and potassium oxide. An ab initio study. Chem Phys 156: 1155–1164

Downs JW (1995) The electron density distribution of coesite. J Phys Chem 99: 6849–6856

Downs JW, Swope RJ (1992) The Laplacian of the electron density and the electrostatic potential of danburite $CaB_2Si_2O_8$. J Phys Chem 96: 4834–4840

Downs RT, Gibbs GV, Boisen MB, Rosso KM (2002) A comparison of procrystal and ab initio model representations of the electron-density distribution of minerals. Phys Chem Miner 29: 369–385

Feth S, Gibbs GV, Boisen MB, Myers RH (1993) Promolecule radii for nitride, oxides and sulfides. A comparison with effective ionic and crystal radii. J Phys Chem 97: 11445–11450

Gatti C (1997) P2DCRY 97 user's manual. CNR-CSRSRC, Milano

Gatti C (1999) TOPOND 98 user's manual. CNR-CSRSRC, Milano

Gibbs GV, Downs JW, Boisen MB (1994) The elusive SiO bond. In: Silica. Heaney PJ, Prewitt CT, Gibbs GV, (eds) HSA, Washington, pp 331–368

Gibbs GV, Hill FC, Boisen Jr MB (1997) The SiO bond and the electron-density distributions. Phys Chem Miner 24: 167–178

Gibbs GV, Boisen MB, Hill FC, Tamada O, Downs RT (1998) SiO and GeO bonded interactions as inferred from the bond critical point properties of electron density distributions Phys Chem Miner 25: 574–584

Gibbs GV, Boisen MB, Rosso KM, Teter DM, Bukowinski MT (2000) Model structures and electron density distributions for silica polymorph coesite at pressure: an assessment of the OO bonded interactions. J Phys Chem (B) 104: 10534–10542

Gibbs GV, Boisen Jr MB, Beverly LL, Rosso KM (2001) A computational quantum chemical study of the bonded interactions in earth materials and structurally and chemically related molecules. In: Cygan RT, Kubicky JD (eds) Molecular modeling theory: application in the geosciences. HSA, Washington, pp 345–381

Gillespie RJ (1972) Molecular geometry. Van Nostrand Reinhold, London

Hoppe R, Voigt S, Glaum H, Kissel J, Muller HP, Bernet K, (1989) A new route to charge distribution in ionic solids. J Less Comm Met 156: 105–122

Kirfel A, Gibbs GV (2000) Electron density distributions and bonded interactions for fibrous zeolites natrolite, mesolite and scolecite and related materials. Phys Chem Miner 27: 270–284

Monkhorst HJ, Pack JD (1976) Special points for Brillouin-zone integration. Phys Rev (B)8: 5188–5192

Nada R, Catlow CRA, Dovesi R, Pisani C (1990) An ab-initio Hartree–Fock study of α-quartz and stishovite. Phys Chem Miner 17: 353–362

Nada R, Catlow CRA, Dovesi R, Saunders VR (1992) An ab initio Hartree-Fock study of the ilmenite-structured $MgSiO_3$. Proc Roy Soc Lond (A)436: 499–509

Newton MD, Gibbs GV (1980) Ab initio calculated geometries and charge distributions for H_4SiO_4 and $H_6Si_2O_7$ compared with experimental values for silicates and siloxanes. Phys Chem Miner 6: 221–246

Ojamae L, Hermansson K, Pisani C, Causà M, Roetti C (1994) Structural vibrational and electronic properties of a crystalline hydrate from ab-initio periodic Hartree–Fock calculations. Acta Crystallogr (B)50: 268–279

Pauling L (1940) The nature of the chemical bond, 2nd ed. Cornell Univ Press, Ithaca

Pisani C, Dovesi R, Roetti C (1988) Hartree–Fock ab-initio treatment of crystalline systems. In: Lecture notes in chemistry UAC, 48. SpringerBerlin, Heidelberg, New York

Prencipe M (2002) Ab initio Hartree–Fock study and charge density analysis of beryl ($Al_4Be_6Si_{12}O_{36}$). Phys Chem Miner 29: 552–561

Saunders VR, Dovesi R, Roetti C, Causà M, Harrison NM, Orlando R, Zicovich–Wilson CM (1998) CRYSTAL98 user's manual. University of Torino, Torino

Shannon RD, Prewitt CT (1969) Effective ionic radii in oxides and fluorides. Acta Crystallogr (B)25: 925–946

Tribaudino M, Nestola F, Prencipe M, Rundlof H (2003) A single-crystal neutron-diffraction investigation of spodumene at 54 K. Can. Mineral 41: 521–527

Tsirelson VG, Avilov AS, Abramov YA, Belokoneva EL, Kitaneh R, Feil D (1998) X-ray and electron diffraction study of MgO. Acta Crystallogr, (B)54: 8–17

Volkov A, Abramov Y, Coppens P, Gatti C (2000) On the origin of topological differences between experimental and theoretical crystal charge densities. Acta Crystallogr (A)56: 332–339

Zhang M, Redhammer GJ, Salje EKH, Mookherjee M (2002) $LiFeSi_2O_6$ and $NaFeSi_2O_6$ at low temperatures: an infrared spectroscopic study. Phys Chem Miner, 29: 609–616